JOURNAL OF MATERIALS SCIENCE 28 (1993) 3529–3538

Yb_2O_3-fluxed sintered silicon nitride

Part I *Microstructure characterization*

J. S. VETRANO, H.-J. KLEEBE, E. HAMPP, M. J. HOFFMANN, M. RÜHLE
Max-Planck Institut für Metallforschung, Institut für Werkstoffwissenschaft, Seestrasse 92, D-7000 Stuttgart 1, Germany

R. M. CANNON
Lawrence Berkeley Laboratory, University of California, Berkeley, CA, USA

Microstructural development and crystallization behaviour of Yb_2O_3-fluxed sintered silicon nitride materials was investigated using CTEM and HREM. The materials contained 5 and 10 vol% Yb_2O_3 as sintering additives. After densification, both compositions were subsequently heat treated to crystallize the residual amorphous secondary phases present at triple-grain regions. In the material doped with 5 vol% Yb_2O_3, only an amorphous secondary phase was observed after sintering, which was about 80% crystalline ($Yb_2Si_2O_7$) after the post-sintering heat treatment. A metastable phase was formed in the material with 10 vol% additives after sintering, with about 70% crystallinity in the triple-point pockets. Upon post-sintering heat treatment, the material could be completely crystallized. During heat treating, the metastable phase combined with the remaining glass to form Yb_2SiO_5 plus $Yb_2Si_2O_7$ and a small amount of Si_3N_4 which deposited epitaxially on pre-existing Si_3N_4 grains in areas of low-energy within the triple-point pockets. All materials contained thin amorphous films separating the grains. The amorphous intergranular films along grain boundaries (homophase boundaries) revealed excess ytterbium and oxygen. The thickness of the intergranular films was about 1.0 and 2.5 nm for the grain boundaries and the phase boundaries, respectively, independent of additive content and heat-treatment history.

1. Introduction

Silicon nitride materials have been intensively studied over many years for their potential application as high-temperature structural ceramics [1–5]. This is due to the favourable combination of chemical and thermo-mechanical properties, e.g. inherently high strength, low coefficient of thermal expansion, and good thermal shock and wear resistance. However, Si_3N_4 cannot be conventionally densified by classical solid-state sintering techniques owing to its high covalent bonding character and low self diffusivity [6, 7]. Therefore, it is commonly processed by liquid-phase sintering using rare-earth or transition-element oxide additives. During sintering, these oxides react with SiO_2 (always present on the surface of the Si_3N_4 grains) and Si_3N_4 to form a liquid that allows both densification of the green body to near theoretical density, and the α- to β-Si_3N_4 transformation to occur [8–10]. This process results in a microstructure consisting of β-Si_3N_4 grains and a small percentage of a secondary phase, consisting usually of silicon, oxygen, nitrogen and cations of the sintering additives. This secondary phase, which is present in both three- and four-grain junctions (pockets) and as a thin amorphous film that forms between essentially all grains (two-grain junctions), is thought to limit the high-temperature properties of the materials [11–15].

The secondary phase is usually amorphous after sintering. Tsuge *et al.* [11] noted that a pre-sintering heat treatment could promote crystallization of triple-grain regions, resulting in an improved high-temperature flexural strength. It should be mentioned that in some cases the crystallization of the secondary phase has been seen to be either detrimental to the high-temperature mechanical properties or not beneficial (especially at room temperature) [16, 17]. This has been attributed to a higher concentration of impurities in the remaining amorphous intergranular phase (i.e. no solid solution with the crystalline phase occurred) and, moreover, to stresses induced in the material due to volume changes upon phase transformation or to thermal expansion mismatch between Si_3N_4 and the crystallized secondary phase. Many different additives have been used to densify silicon nitride, with three factors influencing the choice of the sintering aid: (i) ease of sinterability, (ii) refractoriness of the secondary phase, and (iii) ease of crystallization of the triple-point pockets [18–22]. The most common additives today are Y_2O_3 plus Al_2O_3 which satisfy the first criterion, but it is difficult to obtain complete crystallization of the secondary phase pockets [23–27]. However, by carefully controlling the chemical balance of elements, several researchers have been able to achieve "complete" [28, 29] or nearly complete [30]

0022–2461

crystallization of these pockets. It is important to note that the term "complete crystallization" is used here with the understanding that the aforementioned thin amorphous intergranular films still exist along phase and grain boundaries.

Thin amorphous films are observed between all but low-angle boundaries or special grain boundaries in sintered silicon nitride (SSN) [31] and can range in width from 0.5–5 nm. They are generally assumed to consist mainly of SiO_2 from the surface of the Si_3N_4 grains, though a quantitative chemical analysis of the film has not yet been accomplished due to both interference with adjacent grains and beam broadening during chemical analysis in the electron microscope. The idea that the formation of an amorphous grain-boundary film in some ceramics is an equilibrium phenomenon has been explored by Clarke [32]. He considered attractive and repulsive forces acting on the adjacent grains across the intergranular film and was able to derive a formula which allows, in theory, the calculation of the grain-boundary film thickness. However, some of the parameters involved in the derived equation are still unknown (e.g. the dielectric and elastic constants of the intergranular film and/or the crystalline secondary phase). Hence, a calculation of the equilibrium grain-boundary film thickness in Yb_2O_3-fluxed silicon nitride is not yet possible. Therefore, high-resolution electron microscopy (HREM) has been used to image grain-boundary films in Si_3N_4 materials and to determine the corresponding film width [33, 34].

The present work investigated the microstructural evolution of sintered and annealed silicon nitride fluxed with 5 and 10 vol % Yb_2O_3. The aim of the study was to characterize typical microstructural features of Yb_2O_3-fluxed SSN and compare these with SSN fluxed with other rare-earth oxide additives. This includes the characterization of the crystalline secondary phase and its crystallization behaviour as well as the structure and chemistry of the relatively thin amorphous intergranular films. As the two main creep mechanisms in Si_3N_4-based materials are grain-boundary sliding [35] and solution-precipitation [36], the thickness and viscosity of the amorphous intergranular films are believed to play an important role in the high-temperature mechanical properties of these materials. In Part II [37], the promising mechanical properties of the materials investigated will be presented and correlated with the observed microstructural features.

2. Experimental procedure

The materials investigated were fabricated using 5 and 10 vol % Yb_2O_3 with the addition of 0.5 vol % Al_2O_3 for improved sinterability. The starting powders of Si_3N_4 (E10, UBE Industries, Japan), Yb_2O_3 (Ventron, Germany) and Al_2O_3 (AKP, Sumitomo, Japan) were attrition milled for 4 h in isopropanol and subsequently dried in a rotation evaporator and sieved. The homogeneous powder mixtures were consolidated by cold isostatic pressing at 630 MPa. Sintering was performed in a BN crucible heated by a graphite heating element (Astro Industries, Santa Barbara, USA) with a constant heating rate of 20 K min^{-1} under 1 atm N_2 pressure. The isothermal sintering time at 1800 °C was 120 min which allowed a complete α-β Si_3N_4 transformation, and the attainment of > 99 % theoretical density. The cooling rate in the first stage was about 100 K min^{-1}.

After sintering, each of the materials was heat treated to crystallize the amorphous secondary phase. The optimum temperature for devitrification was determined by DTA investigations with a heating rate of 5 K min^{-1}. The crystallization heat treatment was 12 h at 1250 °C in 1 atm N_2. The sintered and annealed materials were subsequently characterized by transmission electron microscopy (TEM), and X-ray diffraction (XRD) of bulk specimens.

TEM foils were prepared by standard techniques involving cutting slices from the bulk and boring 3 mm discs which were subsequently ground to 100 μm thickness. They were then dimpled to 20 μm and ion milled to perforation. All samples were coated lightly with amorphous carbon to prevent charging in the microscope.

The TEM examinations were performed in either a Jeol 2000 FX (200 kV) with a Tracor EDS system (germanium detector, ultra-thin window), or a Jeol 4000 EX dedicated high-resolution electron microscope (HREM) operating at 400 kV (point resolution of 1.7 nm). High-spatial resolution chemical analysis was carried out in a VG HB 501 STEM using a 0.8 nm probe size.

3. Results

3.1. General microstructure

The general microstructure of all Yb_2O_3-containing materials investigated consisted of elongated β-Si_3N_4 grains, and triple-point pockets filled with remains of the liquid formed during sintering either in amorphous or crystalline form. The triple-grain regions were homogeneously distributed throughout the samples. All Si_3N_4 grains and Si_3N_4/second-phase boundaries were separated by a thin amorphous intergranular film with the only exception of low-energy boundaries or boundaries with special orientation. Table I reveals the crystalline secondary phases that were found in triple-point pockets of each material by both XRD and electron diffraction.

3.1.1. SSN with 5 vol % Yb_2O_3 addition

Virtually all of the triple-point pockets were amorphous in the as-sintered material with 5 vol % Yb_2O_3

TABLE I Crystalline secondary phases determined in Yb_2O_3-doped SSN by XRD and electron diffraction with the second-phase content (estimated by TEM)

Material	Sintered	Heat treated
5 vol % Yb_2O_3	Amorphous 100%	$Yb_2Si_2O_7$ 80%
10 vol % Yb_2O_3	$Yb_{10}Al_2Si_3O_{18}N_4$ 70%	$Yb_2Si_2O_7$ + Yb_2SiO_5 80%

additives. The amorphous triple-grain regions were interconnected by thin amorphous grain-boundary films covering the Si_3N_4 particles. Fig. 1 shows a bright- and diffuse dark-field micrograph of a second-phase pocket that demonstrate its glass structure. Chemical analysis by EDS showed that the glass contained approximately equal amounts of both ytterbium and silicon, a high level of oxygen, but no nitrogen could be detected on the basis of a detection limit of approximately 10 at %, due to the overlap with carbon (carbon coating) and the high amount of oxygen (in the secondary grain-boundary phase).

3.1.2. Heat-treated SSN with 5 vol% Yb_2O_3 addition

After the heat treatment, approximately 80% of the triple-grain pockets were crystalline, either partially or completely. An example of a completely crystallized secondary-phase pocket can be seen in Fig. 2. Both XRD and selected-area diffraction (SAD) indicated that the secondary crystalline phase was $Yb_2Si_2O_7$. Quantitative EDS analysis confirmed a Yb:Si ratio of 1:1. The Si_3N_4-rich corner of the Si_3N_4–Yb_2O_3–SiO_2 phase diagram, indicating both starting compositions investigated, is shown in Fig. 3 [38]. The composition of the materials with 5 vol % Yb_2O_3 lies in the Si_3N_4–Si_2N_2O–$Yb_2Si_2O_7$ compatibility triangle, but no Si_2N_2O could be detected by XRD or electron microscopy. Huang *et al.* [39] reported the thermal decomposition of Si_2N_2O at elevated sintering temperatures of 1830 °C into Si_3N_4 and SiO_2. Moreover, nucleation difficulties may influence the absence of Si_2N_2O in this material. It was reported by Braue [40] and Kleebe *et al.* [41] that Si_2N_2O particles typically reveal spherical inclusions which were identified as α-Si_3N_4 acting as a nucleation site during the formation of Si_2N_2O. The incomplete crystallization of the $Yb_2Si_2O_7$ secondary phase after the post-sintering heat treatment is not yet well understood but it should be noted that recent calculations have shown that internal stresses in Si_3N_4-materials, due to large volume changes upon crystallization, may limit complete crystallization of the triple-grain pockets [42, 43].

3.1.3. SSN with 10 vol% Yb_2O_3 addition

The microstructure of the material with 10 vol % Yb_2O_3 additives was substantially different compared to the material with 5 vol % Yb_2O_3 addition. After sintering, already a large amount of the secondary phase had crystallized in the triple points. This phase, tentatively identified as $Yb_{10}Al_2Si_3O_{18}N_4$ by both XRD and EDS, existed as large grains extending up to several micrometres in size, similar to those seen in other SSN materials [44]. An example of one such crystal of the interconnected secondary phase network is shown in the transmission electron micrographs of Fig. 4. The exact identification of this phase was hampered by the lack of data in the appropriate Yb_2O_3-based phase diagrams, but the lattice spacings as measured by X-ray diffraction were close to the yttrium equivalent of this phase $Y_{10}Al_2Si_3O_{18}N_4$ [45], and the measured Yb:Si ratio of 10:3 matched well. Owing to the large amount of ytterbium in this phase, the aluminium content could not be measured quantitatively by EDS as the AlK_α peak and the YbM_α overlap (1.487 and 1.521 keV, respectively). However, using a peak subtraction routine with a $Yb_2Si_2O_7$ standard yielded a small aluminium peak for the secondary phase.

Although the individual triple-point pockets, as seen in the TEM, showed various degrees of crystallinity after sintering, the overall amount of crystalline

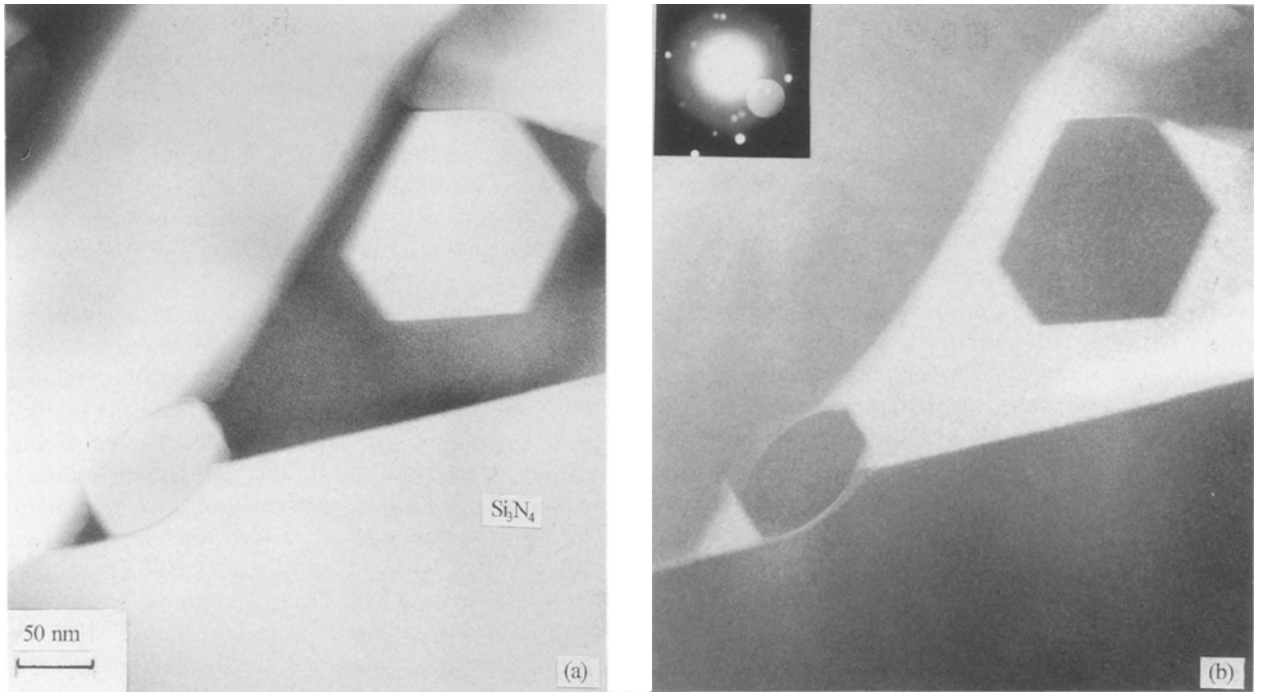

Figure 1 Transmission electron micrographs of a second-phase pocket in the 5 vol % Yb_2O_3-fluxed sintered sample using (a) bright-field and (b) diffuse dark-field imaging, indicating that the secondary phase is completely amorphous.

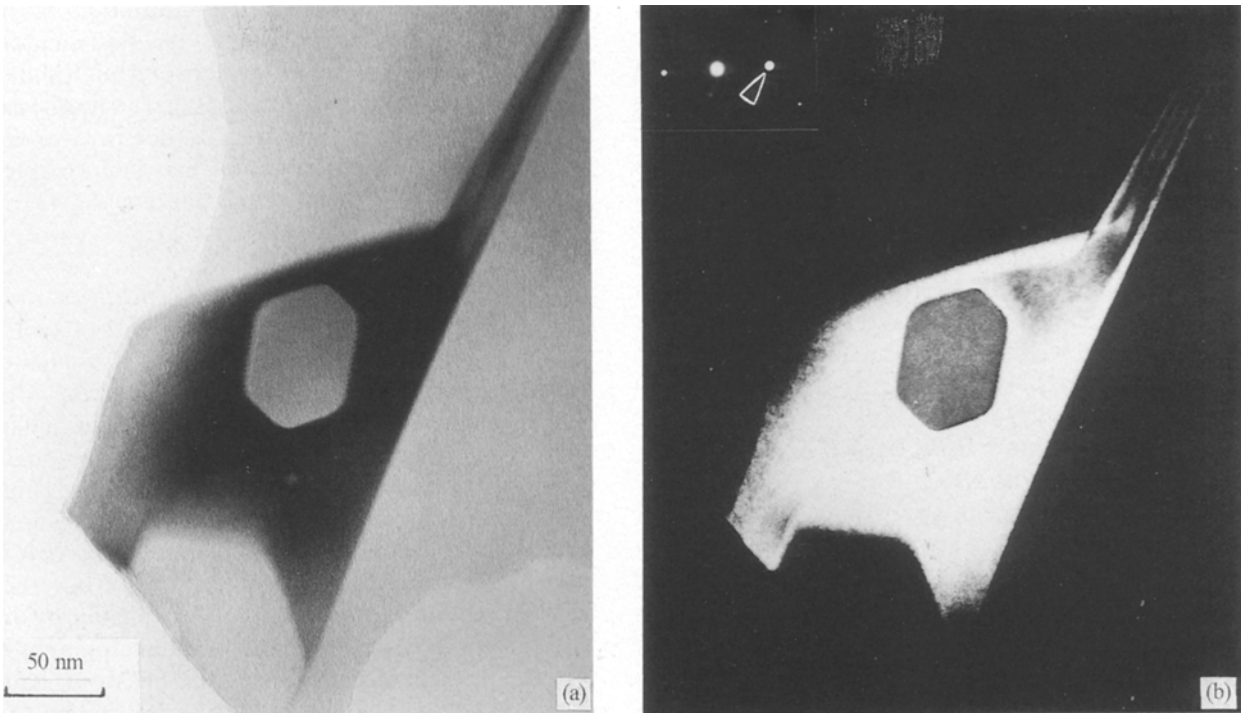

Figure 2 Micrographs of a second-phase pocket in the 5 vol % Yb_2O_3-fluxed heat-treated sample showing complete crystallinity in (a) bright-field and (b) dark-field. Diffraction spot used for imaging of the secondary phase is indicated.

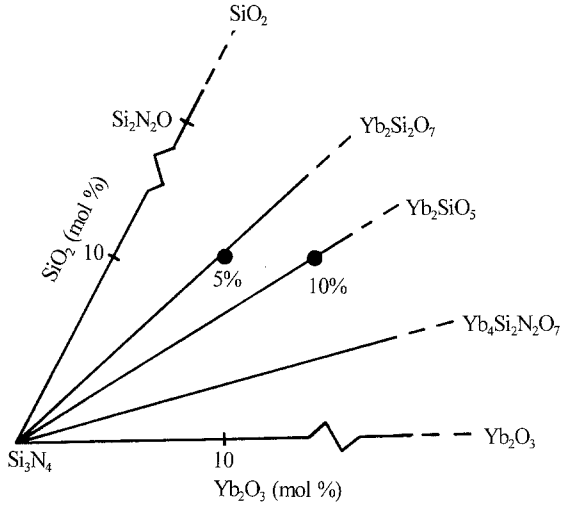

Figure 3 Si_3N_4–Yb_2O_3–SiO_2 phase diagram indicating the positions of the two starting compositions investigated.

secondary phase was approximately 70%. In triple-grain pockets that were partially crystalline the growth front often appeared planar, as can be seen from the micrographs in Fig. 5, indicating that the crystallization was probably stopped by the rapid cooling of the sample. The remaining glass contained about equal atomic amounts of ytterbium and silicon. Another possible explanation for the observed planar growth fronts is related to the chemical composition of the residual glass. Upon crystallization of the secondary phase, a SiO_2-enriched glass is formed (ytterbium depletion; Yb:Si ratio of the crystalline phase = 10:3 and of the amorphous material = 1:1) which may inhibit further crystallization as the chemical composition changed.

3.1.4. Heat-treated SSN with 10 vol % Yb_2O_3 addition

TEM examination of the 10 vol % Yb_2O_3 containing material after a post-sintering heat treatment showed that the secondary phase material in the triple points was completely crystallized. More specifically the pockets were, almost without exception, crystallized all the way into the "corners" formed by the Si_3N_4 grains. This is contrary to the calculations of Raj and Lange [43], who reported on the impossibility to completely crystallize a second-phase pocket due to the increase of hydrostatic stresses during crystallization. However, they assumed that the material could support a hydrostatic stress which might not be valid for the applied heat-treatment temperature of 1250 °C which is above the T_g of 1120 °C for pure silica glass. Moreover, internal stresses can be relaxed via viscous flow of the amorphous phase and/or by solution–reprecipitation processes along the grain boundaries [42].

The previously large secondary-phase particles extending over several triple pockets observed in the as-sintered microstructure were broken up into smaller grains; often more than one grain forming per pocket. Not surprisingly, given the non-steady-state conditions of crystallization in the as-sintered samples, there was also a phase change upon heat treatment. The new secondary phase formed after heat-treating was Yb_2SiO_5 with an additional small amount of about 20% of the $Yb_2Si_2O_7$ second phase. The formation of these two phases is in accordance with the starting compositions in the Si_3N_4–Yb_2O_3–SiO_2 phase diagram as shown in Fig. 3. It should be pointed out that this is markedly different from the Y_2O_3-based phase diagram. In the ytterbium-containing

Figure 4 (a) Dark-field, and (b) bright-field micrograph showing large second-phase crystals of the same orientation in the as-sintered material with 10 vol % additives.

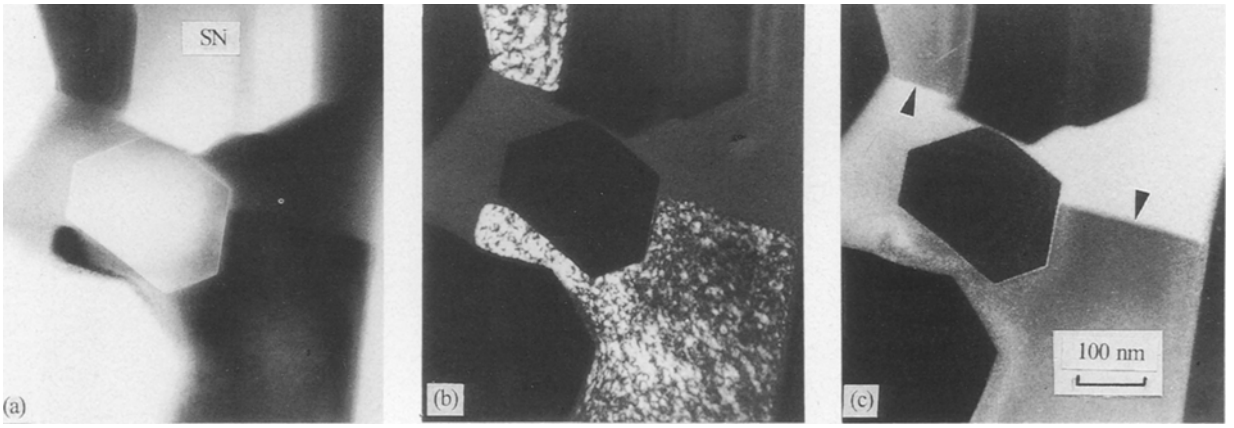

Figure 5 (a) Bright-field, (b) dark-field and (c) diffuse dark-field images of a second-phase pocket in the 10 vol % Yb_2O_3 as-sintered specimen illustrating a partially crystalline pocket with planar growth fronts (arrowed).

system the ytterbium apatite phase $Yb_{10}(SiO_4)_6N_2$ is missing, resulting in a compatibility triangle with Si_3N_4 and the two ytterbium silicates Yb_2SiO_5 and $Yb_2Si_2O_7$ as described above (Fig. 6). When more than one second-phase grain was present in a pocket, they were separated by a thin amorphous intergranular film. This is apparent in the transmission electron micrographs of Fig. 7 where the bright- and diffuse dark-field images show the grain boundaries in the triple-point pocket and the amorphous film between the two secondary-phase grains, respectively. Chemical analysis by EDS indicated that neighbouring second-phase grains were often the same phase, but not necessarily. In addition, electron diffraction studies showed no crystallographic orientation relationship between the different secondary-phase grains filling one pocket.

Two most striking microstructural features in the heat-treated material with 10 vol % Yb_2O_3 addition were (i) the rounding of the triple-point corners, as seen in Fig. 8, and (ii) the "bumps" on the Si_3N_4 grains at second-phase grain-boundary intercepts shown in Fig. 7. EDS analysis revealed the material forming these features to be silicon nitride deposited on the

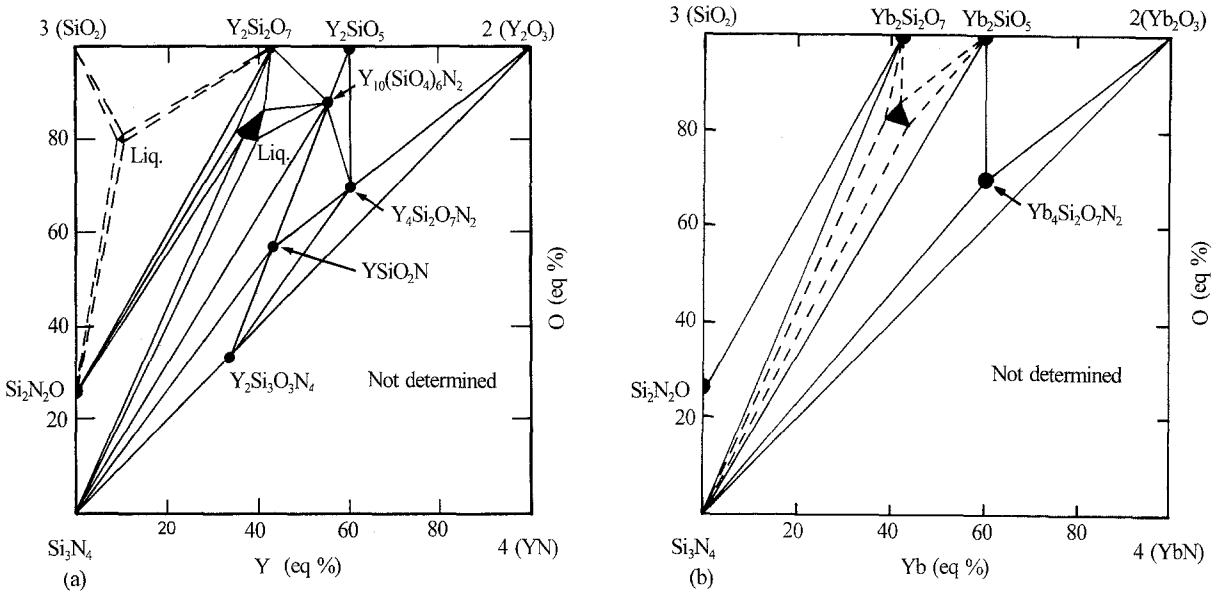

Figure 6 Comparison between the (a) Si_3N_4–Y_2O_3–SiO_2 [55] and (b) the Si_3N_4–Yb_2O_3–SiO_2 phase diagram [38] (note that in the Yb_2O_3 system the apatite phase is missing).

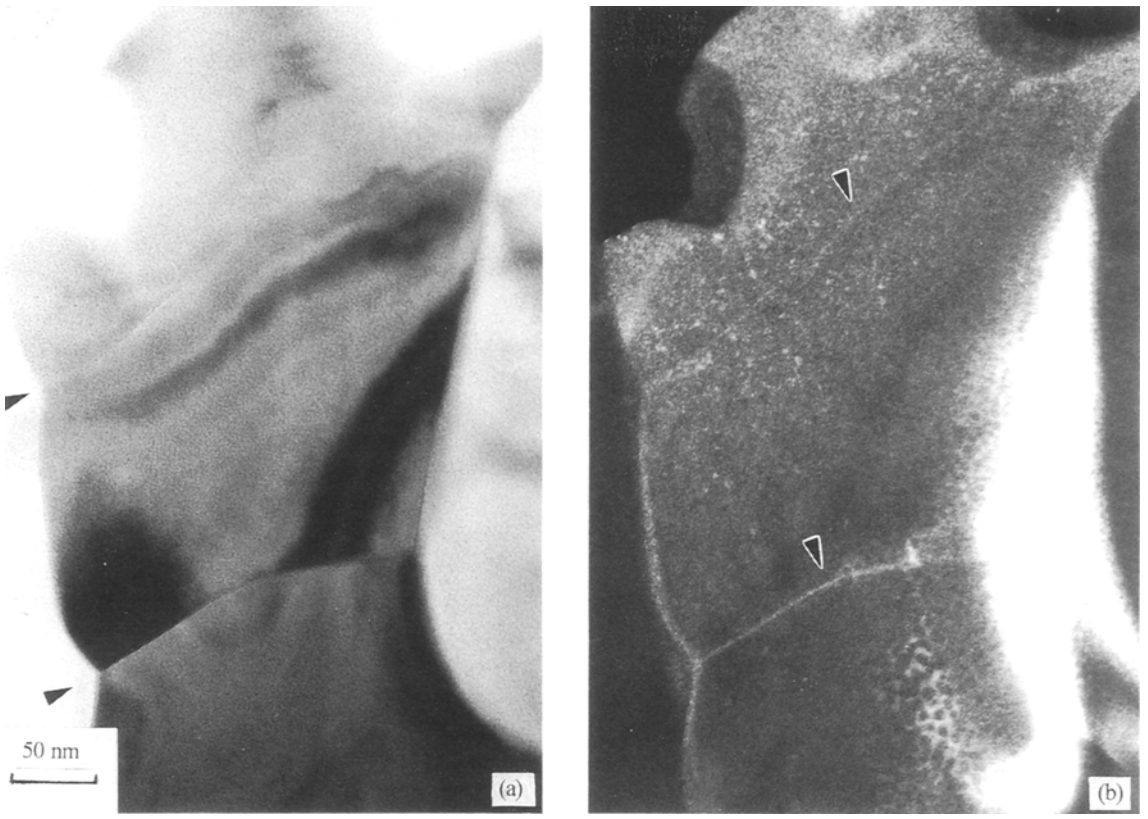

Figure 7 (a) Bright-field and (b) diffuse dark-field micrographs demonstrating the multigrain second-phase pockets present in the material with 10 vol % additives, after a post-sintering heat treatment. The "bumps" on the Si_3N_4 grains at the second-phase grain boundary are arrowed in (a), and the thin amorphous layer between the Si_3N_4 and secondary phase grains, and between the two secondary phase grains can be seen in (b).

matrix grains. HREM indicated that the depositions were epitaxial with the "parent" Si_3N_4 grains. As these features were not observed in the as-sintered microstructure, and the chemistry of the newly formed crystalline secondary phases indicates that silicon and nitrogen must be rejected from the triple-point pockets during annealing, it is postulated that these features are formed by Si_3N_4 deposited epitaxially during the heat-treatment process [46].

3.2. Grain-Boundary films

All of the materials examined contained thin amorphous intergranular films that surrounded virtually all grains. The non-crystallinity of these films has been confirmed using different techniques, e.g. HREM, diffuse dark-field imaging, and the appearance of Fresnel fringes in over- and under-focused conditions [47–49]. The width of such films was seen to vary according to the two grains that it separated; being the

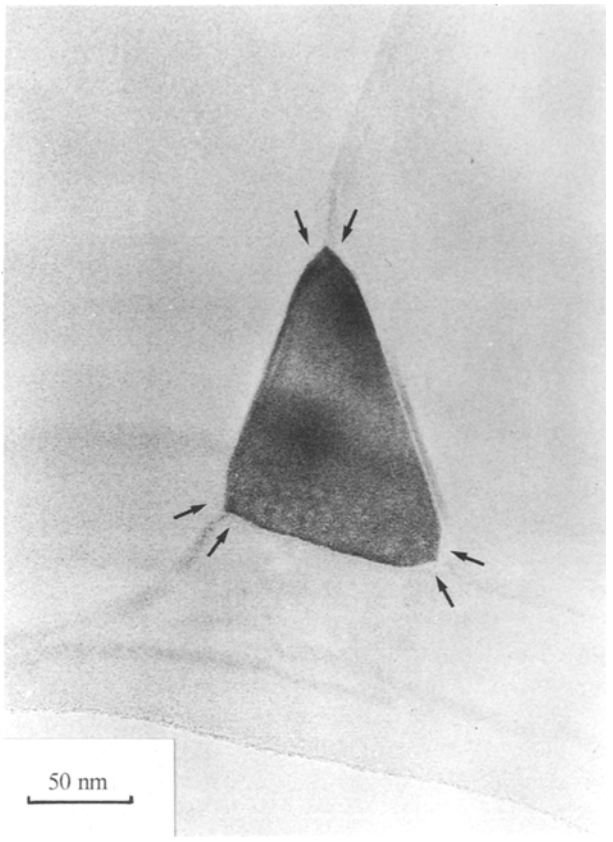

Figure 8 Rounded corners of a second-phase pocket, typical in the material with 10 vol % additives after a post-sintering heat treatment, due to the epitaxial deposition of Si_3N_4.

thinnest when the two grains were the same material ("homophase" boundary, Fig. 9a) and the widest in the case of dissimilar grains ("heterophase" boundary, Fig. 9b). However, for a given boundary type, the width of the film was seen to be constant with values of about 1.0 ± 0.1 and 2.5 ± 0.2 nm for the homogeneous and heterogeneous boundaries, respectively. It should be noted that the film thickness in the homophase boundary was the same for all materials investigated, regardless of the amount of additives or the heat-treatment history. Most importantly, the measured film width is relatively thin compared to Si_3N_4 fluxed with other rare-earth oxides [50]. The assumption that these boundary widths are of equilibrium thickness is supported by two observations: (i) the thickness of a homophase boundary film is constant, even when the two Si_3N_4 grains are interpenetrating, and (ii) the thickness of the heterophase boundary film is also constant in the region around the newly deposited Si_3N_4 (Fig. 8). If these films were not of an equilibrium thickness, the width would be expected to vary in the observed situations of high stress (interpenetrating grains) or strong chemical activity (epitaxial deposition).

The chemistry of an intergranular film along the homophase boundary was investigated by EDS in a dedicated STEM utilizing a 0.8 nm probe size. The film was found to contain both excess ytterbium and oxygen. The presence of ytterbium was most striking between the silicon nitride grains as the heavy element absorbs more electrons, causing the film to stand out as a dark line in the TEM. This is shown in the bright-field micrograph of Fig. 10 of a grain-boundary film between two Si_3N_4 grains, indicated by the dark line extending from a triple-point pocket in the upper right. The accompanying EDS spectra illustrate the presence of ytterbium and oxygen at the grain boundary compared to a measured point 8.0 nm into one Si_3N_4 grain. The silicon or nitrogen content in the homophase boundary film could not be evaluated quantitatively due to interference from the surrounding Si_3N_4 grains. The chemical composition of the heterophase boundary films could not be measured due to the interference with the Si_3N_4 grains and the ytterbium-containing crystalline secondary phases.

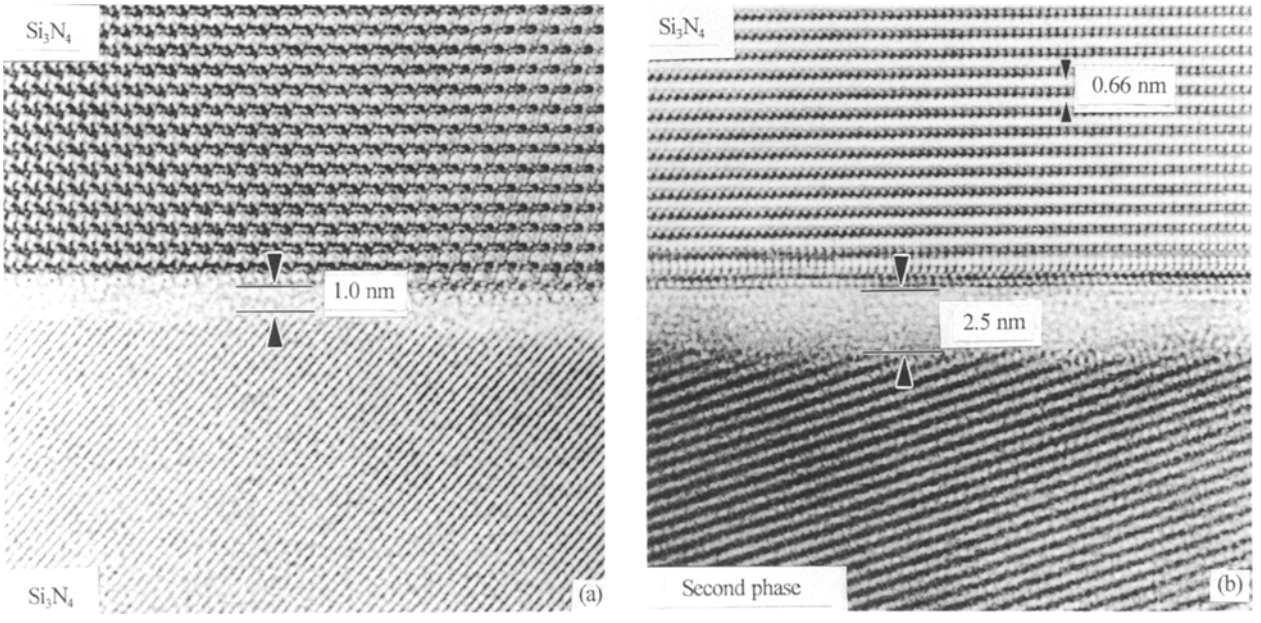

Figure 9 HREM micrographs demonstrating the amorphous layer (a) between two Si_3N_4 grains and (b) between a Si_3N_4 and a secondary phase grain. Note that the "heterophase boundary" (shown in b) is substantially wider (1.0 and 2.5 nm, respectively).

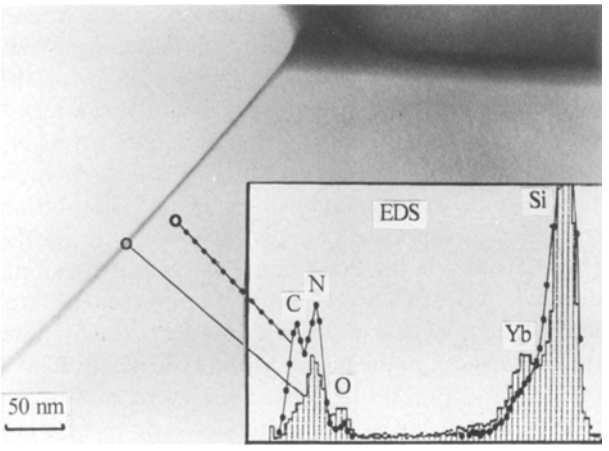

Figure 10 Transmission electron micrograph showing the dark line between Si_3N_4 grains, indicating the presence of ytterbium in the thin amorphous film, and EDS spectra from the grain boundary and 8.0 nm into the Si_3N_4 grain, confirming it. Also note the presence of oxygen in the film. The carbon signal is due to the carbon coating on the sample.

4. Discussion

The use of Yb_2O_3 as a sintering agent for Si_3N_4 components appears to have strong potential for high-temperature applications, judging by the microstructural features observed in TEM. The two most important characteristics of the ytterbium-fluxed SSN materials studied are (i) the ease of crystallization of the secondary phase, as seen by the large degree of devitrification in the 10 vol % Yb_2O_3 containing sample even before heat treatment, and (ii) the presence of ytterbium in the thin amorphous grain- and phase-boundary films.

The complete crystallization of secondary phases in SSN has been a goal since the findings of Tsuge *et al.* [11], and it is therefore significant that the secondary phases formed in the Y_2O_3-fluxed materials crystallize so easily and completely. SSN materials fluxed with other rare-earth oxide additives (e.g. Yb_2O_3 + Al_2O_3) have proved more difficult to crystallize completely [8–15]. However, in the material doped with 5 vol % Yb_2O_3, a post-sintering heat treatment did not achieve complete crystallization, but even some small pockets, which usually remain amorphous in other systems, were completely crystalline. It is not yet well understood why the crystallization behaviour of Yb_2O_3-containing materials differs from other systems, but two possible explanations can be proposed. First, it is possible that the ytterbia silicates have some solid solution with the impurity atoms (i.e. calcium and iron) that are usually present and are often assumed to be heavily concentrated in the remaining amorphous material, preventing complete crystallization. Second, it is also possible that the amorphous material in the Yb_2O_3-fluxed material undergoes only a small volume change on crystallization, thereby reducing the internal stresses that can accumulate and may hinder further devitrification. The properties of the crystalline phases in this system are currently under investigation to try to answer some of these questions. Moreover, the close chemical composition of the amorphous phase and the crystalline ytterbium silicate formed regarding the Yb:Si ratio may also support a more complete degree of devitrification.

The relative ease of crystallization throughout the 10 vol % Yb_2O_3-fluxed material over the 5 vol % containing samples is probably due to the large interconnection of triple-point pockets in the material with the higher additive content. In the material with 5 vol % Yb_2O_3 the pockets are more isolated from each other (except for the thin films at two-grain junctions), or it can be thought of as having a smaller average channel size between three-grain junctions compared to the 10 vol % sample. If this channel size is smaller than is required to move a crystallization front through, each triple-point pocket must have its own crystallization nucleus. The large grain size of the metastable secondary phase present in the as-sintered sample with 10 vol % Yb_2O_3 indicates that nucleation events are rare in this condition. Therefore, very little crystallization would be expected if the pockets are isolated. The larger channels in the 10 vol % Yb_2O_3-fluxed material also ease the transport of cations or anions ahead of the crystallization front, which is required if the crystalline phase is not the same composition as the original glass. During the post-sintering heat treatment the nucleation probability is high, as indicated by the crystallization of many triple-point pockets in the 5 vol % sample, and the small grain size of the secondary phases in the pockets of the 10 vol % sample.

The reason for the crystallization of a metastable phase in the material with 10 vol % Yb_2O_3 is not known, but in both the 5 and 10 vol % heat-treated samples the phases present are in line with the equilibrium phase diagram. One possible explanation is that the metastable phase is easier to nucleate, or is only stable at the high sintering temperature where it formed, but at the heat-treatment temperature (1250 °C) the ytterbium silicates nucleate and grow in accordance with the phase diagram. The absence of Si_2N_2O in the Yb_2O_3-doped materials is not surprising, as it generally requires α-Si_3N_4 to nucleate [40, 41]. Moreover, it is believed that a slightly higher additive concentration would result in 100% crystallization of $Yb_2Si_2O_7$.

It should also be noted that the secondary phases formed after heat treatment are, for both additive compositions, oxides, which are expected to fare well in an oxidizing environment. The oxidation of secondary oxynitride phases has been seen to have deleterious effects on the mechanical properties due to the large volume change when these phases convert to oxides [51, 52]. Therefore, in this material no cracking due to a secondary-phase change during service at high temperature in an oxygen-containing environment should occur. However, in the material with 10 vol % Yb_2O_3 addition after heat treatment the following reaction can occur

$$Yb_2SiO_5 + SiO_2 \rightarrow Yb_2Si_2O_7 \quad (1)$$

resulting in a volume change which can cause the formation of internal stresses [12].

The presence of ytterbium in the amorphous intergranular films is interesting and probably beneficial

for the retention of the mechanical properties at high service temperatures. Ytterbium was also found in the grain-boundary films of a commercially available ytterbia-fluxed silicon nitride material, which exhibited very good high-temperature flexural strength and good creep resistance [53]. As the viscosity of pure amorphous Yb_2O_3 is not known, and because of interference from the Si_3N_4 grains on either side of the film, the silica content and exact chemistry of such films could not be determined. It is suspected that cations of additives are also present in the thin amorphous films in other silicon nitride materials but they are generally difficult to detect because the film is so narrow. However, it was reported recently that cerium could be detected qualitatively in the intergranular films of a ceria-fluxed SSN material [54].

One of the most interesting aspects in this system is the epitaxial deposition of Si_3N_4 on pre-existing grains. The evolution of this microstructural feature has already been outlined in detail elsewhere [43], but the general process is the deposition, during the post-sintering heat treatment, of excess silicon and nitrogen from both the glass and the pre-existing crystalline secondary phase due to a change in second-phase composition. This is the first direct evidence for the occurrence of the epitaxial deposition process. The reason that it is more apparent in this system is probably due to the presence of the (non-equilibrium) crystalline phase before the heat treatment. This prevents the silicon and nitrogen from depositing evenly over existing Si_3N_4 grains because of the necessity of maintaining the equilibrium thickness of the amorphous film between the Si_3N_4 and the second-phase grains. They must then deposit on areas of lower energy, e.g. the triple-point "corners" where crystallization was not complete, or near the newly formed grain boundaries in the secondary phase.

5. Conclusion

A systematic study of the microstructural development in combination with the crystallization behaviour in Yb_2O_3-fluxed sintered silicon nitride is reported. The material with 5 vol % additive contained only an amorphous secondary phase after sintering. The second-phase material was about 80% crystalline in the form of $Yb_2Si_2O_7$ after a post-sintering heat treatment. Utilizing 10 vol % additives, a metastable phase was formed after sintering, with about 70% crystallinity in the triple-point pockets. The second-phase pockets were interconnected forming a three-dimensional network. After post-sintering heat treatment, this metastable phase combined with the residual glass to form Yb_2SiO_5 plus $Yb_2Si_2O_7$ and a small amount of Si_3N_4 which deposited epitaxially on pre-existing Si_3N_4 grains. The triple-point pockets were completely crystallized in the 10% heat-treated material, with the exception of a thin amorphous layer between the grains. The amorphous intergranular films present in all materials investigated contained excess ytterbium and oxygen. The thickness of these films was about 1.0 nm, independent of additive content and heat treatment, for the grain boundaries (Si_3N_4/Si_3N_4) and about 2.5 nm for the phase boundaries (Si_3N_4/secondary phase).

Acknowledgement

We thank the BMFT for support under the contract numbers NTS 0230/0 and 03 M 2012.

References

1. C. A. ANDERSON and R. J. BRATTON, "Ceramics Materials for High Temperature Turbines", Final Report, ERDA, AC-05-760-90405 (1977).
2. F. L. RILEY, "Progress in Nitrogen Ceramics", in Proceedings of the NATO Advanced Study Institute on Nitrogen Ceramics, Brighton, 1981 (Martinus Nijhoff, 1983).
3. J. J. BURKE, E. N. LENOE and R. N. KATZ, "Ceramics for High Performance Applications", Vols I–III (Brook Hill, Chestnut Hill, MA, 1974, 1977, 1980).
4. S. SOMIYA, E. KANAI and K. ANDO, in "Proceedings of the 1st International Symposium on Ceramic Components for Engines" edited by F. L. Riley (KTK Scientific, Tokyo, 1983).
5. W. BUNK and M. BÖHMER, "Keramische Komponenten für Fahrzeug-Gasturbinen", Vols I–III (Springer, Berlin, 1977, 1980, 1984).
6. K. KIJIMA and S. SHIRASAKI, *J. Chem. Phys.* **65** (1976) 2668.
7. C. D. GRESKOVICH, S. PROCHAZKA and J. H. ROSOLOWKI, in "Nitrogen Ceramics", edited by F. L. Riley (Nordhoff, Leyden, 1977) pp..351–7.
8. M. MITOMO, M. TSUTSUMI, E. BANNAI and T. TANAKA, *Amer. Ceram. Soc. Bull.* **55** (1976) 313.
9. G. R. TERWILLIGER and F. F. LANGE, US Pat. 3992 497 (1976).
10. A. GIACHELLO, P. C. MARTINENGO, G. TOMMASINI and P. POPPER, *J. Mater. Sci.* **14** (1979) 2825.
11. A. TSUGE, K. NISHIDA and M. KOMATSU, *J. Amer. Ceram. Soc.* **58** (1975) 323.
12. F. F. LANGE, *Amer. Ceram. Soc. Bull.* **62** (1983) 1369.
13. G. N. BABINI, A. BELLOSI and P. VINCENZINI, *Ceram. Int.* **6** (3) (1980) 91.
14. D. R. CLARKE, F. F. LANGE and G. D. SCHNITTGRUND, *J. Amer. Ceram. Soc.* **65** (1982) C-51.
15. W. A. SANDERS and D. M. MIESKOWSKI, *ibid.* **64** (1985) 304.
16. L. A. PIERCE, D. M. MIESKOWSKI and W. A. SANDERS, *J. Mater. Sci.* **21** (1986) 1345.
17. N. HIROSAKI, A. OKADA and K. MATOBA, *J. Amer. Ceram. Soc.* **71** (1988) C-144.
18. R. W. RICE and W. J. McDONOUGH, *ibid.* **58** (1975) 264.
19. H.-J. KLEEBE, G. WÖTTING and G. ZIEGLER, *Sci. Ceram.* **14** (1987) 407.
20. L. K. L. FALK and M. HOLMSTRÖM, in "Euro-Ceramics 1", edited by G. de With, R. A. Terpstra and R. Metselaar (Elsevier Applied Science, London, 1989) pp. 373–7.
21. J. R. KIM and C. H. KIM, *J. Mater. Sci.* **25** (1990) 493.
22. T. EKSTRÖM, L. K. L. FALK and E. M. KNUTSON-WEDEL, *J. Mater. Sci. Lett.* **9** (1990) 823.
23. G. R. TERWILLIGER, *J. Amer. Ceram. Soc.* **57** (1974) 48.
24. D. R. CLARKE and G. THOMAS, *ibid.* **61** (1978) 114.
25. R. E. LOEHMAN and D. J. ROWCLIFFE, *ibid.* **6** (1980) 144.
26. R. K. GOVILA, *J. Mater. Sci.* **20** (1985) 4345.
27. E. TANI, M. NISHIJIMA, H. ICHINOSE, K. KISHI and S. UMEBAYASHI, *Yogyo-Kyokai-Shi* **94** (1986) 300.
28. L. K. L. FALK and G. DUNLOP, *J. Mater. Sci.* **22** (1987) 4369.
29. M. K. CINIBULK, G. THOMAS and S. M. JOHNSON, *J. Amer. Ceram. Soc.* **73** (1990) 1606.
30. D. A. BONNELL, T. Y. TIEN and M. RÜHLE, *ibid.* **70** (1987) 460.
31. H. SCHMID and M. RÜHLE, *J. Mater. Sci.* **19** (1984) 615.
32. D. R. CLARKE, *J. Amer. Ceram. Soc.* **70** (1987) 15.
33. H.-J. KLEEBE, *J. Europ. Ceram. Soc.* **10** (1991) 151.

34. D. R. CLARKE, *J. Amer. Ceram. Soc.* **72** (1989) 1604.
35. R. L. TSAI and R. RAJ, *ibid.* **63** (1980) 513.
36. R. RAJ, *J. Geophys. Rev. B* **87** (1982) 4731.
37. E. HAMPP, M. J. HOFFMANN, H.-J. KLEEBE, J. S. VETRANO and G. SCHNEIDER, *J. Mater. Sci.* (1993) submitted.
38. E. HAMPP, J. GRÖBNER, M. J. HOFFMANN and G. PETZOW, to be published.
39. Z. K. HUANG, P. GREIL and G. PETZOW, *Ceram. Int.* **10** (1984) 14.
40. W. BRAUE, *Mater.-wiss. Werkstoff.* **21** (1990) 72.
41. H.-J. KLEEBE, W. BRAUE, W. LUXEM and M. RÜHLE, in "Proceedings of 4th International Symposium on Ceramic Materials and Components for Engines", Swedish Ceramic Society, 10–12 June 1991, Göteborg, Sweden.
42. H. KEßLER, H.-J. KLEEBE, R. W. CANNON and W. POMPE, *Acta Metall.* (1991) submitted.
43. R. RAJ and F. F. LANGE, *Acta Metall.* **29** (1981) 1993.
44. D. A. BONNELL, *Mater. Sci. Forum* **47** (1989) 132.
45. R. R. WILLS, *J. Amer. Ceram. Soc.* **58** (1975) 335.
46. J. S. VETRANO, H.-J. KLEEBE, E. HAMPP, M. J. HOFFMANN and R. M. CANNON, *J. Mater. Sci. Lett.* **11** (1992) 1249.
47. D. R. CLARKE, *Ultramicroscopy* **4** (1979) 33.
48. J. N. NESS, W. M. STOBBS and T. F. PAGE, *Phil. Mag. A* **54** (1986) 679.
49. O. L. KRIVANEK, T. M. SHAW and G. THOMAS, *J. Appl. Phys.* **50** (1979) 4223.
50. H.-J. KLEEBE, J. S. VETRANO, J. BRULEY and M. RÜHLE, in "Proceedings of 49th Annual EMSA Meeting", 4–9 August, San Jose, edited by G. W. Bailey (San Francisco Press, 1991) p. 930.
51. F. F. LANGE, *J. Amer. Ceram. Soc.* **63** (1980) 38.
52. J. K. PATEL and D. P. THOMPSON, *Brit. Ceram. Trans. J.* **87** (1988) 70.
53. M. J. HOFFMANN, E. HAMPP, J. S. VETRANO, H.-J. KLEEBE and G. PETZOW, to be published.
54. H.-J. KLEEBE and M. K. CINIBULK *J. Mater. Sci. Lett.* **12** (1993) 70.
55. L. J. GAUCKLER, H. HOHNKE and T. Y. TIEN, *J. Amer. Ceram. Soc.* **63** (1980) 35.

Received 27 February
and accepted 10 December 1992